La and Ca-Doped A-site Deficient Strontium Titanates Anode for Electrolyte Supported Direct Methane Solid Oxide Fuel Cell

Pankaj Kr. Tiwari[a], Xiangling Yue[b], John TS Irvine[b], Suddhasatwa Basu[a]*

[a] Department of Chemical Engineering, Indian Institute of Technology Delhi
New Delhi 110016, India
[b] School of Chemistry, University of St. Andrews, Fife KY16 9ST, Scotland, UK

*Corresponding author, email: sbasu@iitd.ac.in; Tel. 91 11 26591035

Abstract

Nickel-yttria stabilized zirconia (Ni-YSZ) cermet anodes for solid oxide fuel cells (SOFC) possesses excellent catalytic properties and stability for H_2 oxidation but not for hydrocarbons as it results in fast carbon deposition in absence of excess steam. In the present work, A-site deficient porous $LSCT_{A-}$ ($La_{0.2}Sr_{0.25}Ca_{0.45}TiO_3$) anode has been fabricated using the environment friendly, aqueous tape casting method followed by the same procedure for the dense YSZ electrolyte and YSZ porous scaffold as cathode matrix. The anode, electrolyte, and porous cathode matrix have been laminated together and sintered up to 1350 ℃. After sintering, nitrate precursors of La, Sr, Co and Fe are infiltrated inside the porous YSZ cathode matrix to form the perovskite phases of $La_{0.8}Sr_{0.2}CoO_3$ (LSC) and $La_{0.8}Sr_{0.2}FeO_3$ (LSF). The as fabricated electrolyte supported SOFCs have been tested in H_2 and CH_4 fuel at 800 ℃. The electrolyte supported cell 15%LSF-5% LSC-YSZ/YSZ/4%Ni-6 %CeO$_2$-$LSCT_{A-}$ gives maximum power density of 328 mW cm^{-2} for 3 h in H_2, but in CH_4 the performance decreased to 165 mW cm^{-2} even though a sustained open circuit voltage of ~1V obtained during H_2 and CH_4 operation. The morphology of the anode before and after cell testing has been analyzed using scanning electron microscope followed by X-ray diffraction studies to understand phase changes during fabrication and testing.

Key Words: A-site deficient $SrTiO_3$, Direct Methane SOFC, $LSCT_{A-}$ anode.

Introduction

Sintering of nickel (Ni) particles at elevated temperature and coke formation in hydrocarbon fuels restrict the application of nickel-yttria stabilized zirconia (Ni-YSZ) composite anode matrices in a solid oxide fuel cell (SOFC). The development of anode catalyst for direct hydrocarbon SOFC with improved electrochemical properties and durability remains as a major concern towards its commercialization. Alternative anode materials such as copper-ceria-YSZ have been developed, which significantly reduces coke formation[1-3]. Thermal instability and poor electrochemical activity of copper-ceria-YSZ anodes at the SOFC operation temperature (>700 °C) necessitates the use of new strategies to improve the performance of anodes fed with hydrocarbon, e.g., methane, n-propane and n-butane directly [4-8]. Earlier it was shown that Ni coarsening can be prevented due to sintering by using strong metal support interaction between Ni and other transition metal oxides (TMO) e.g., TiO_2, CeO_2, Nb_2O_5 [9-12]. Strontium titanate ($SrTiO_3$) has been proven to be a potential alternative to Ni based anode as it possesses desirable thermal and chemical stability and shows mixed ionic and electronic conducting (MIEC) behavior at low oxygen partial pressure as well as restricting coke formation[13-15]. $SrTiO_3$ perovskite structure has stability and flexibility to incorporate cations with variable oxidation states, which in turn provides enhanced electrocatalytic property and electronic conductivity. Ti^{4+}/Ti^{3+} redox couple in the reducing atmosphere can accept electrons from hydrocarbon or H_2 and promote dissociation. Oxygen-2p orbital and the empty conduction band from titanium-3d orbitals constitute the electronic energy band of $SrTiO_3$. Doping with trivalent atoms such as La^{3+} and Y^{3+} in place of Sr^{2+} makes it n-type semiconductor having higher electrical conductivity than the pure $SrTiO_3$ (ST). In order to maintain the electroneutrality, the substitution of Sr^{2+} with La^{3+} can be compensated by introducing the extra oxygen beyond the ABO_3 stoichiometry under oxidizing conditions, defined as 'oxygen excess' $La_xSr_{1-x}TiO_{3+x/2}$ or creating A-site vacancies, as $La_xSr_{1-3x/2}TiO_3$,

'A-site deficient'. Lanthanum is an appropriate donor dopant because its ionic radius is similar to that of Sr^{2+}. Doping at A-site or B-site in $SrTiO_3$ improves the electrical and ionic conductivity of the system[16]. It has been reported that reduced $La_{0.2}Sr_{0.7}TiO_3$ (LST_{A-}) gives high electronic conductivity of 39.75 S cm^{-1} at 700 °C[17]. It may also be noted that lanthanum and yttrium-doped $SrTiO_3$ do not undergo solid state reactions with YSZ even after sintering at 1450 °C[18] and hence suitable to use as an anode with YSZ as the electrolyte.

The introduction of calcium (Ca) into LST_{A-} decreases the unit cell volume and facilitates the reduction of fuel[16]. Calcium doping also helps in lowering the sintering temperature of LST_{A-} backbone. It has been reported that Ca doped LST_{A-} ($La_{0.20}Sr_{0.25}Ca_{0.45}TiO_3$) gives maximum electronic conductivity of 27.53 S cm^{-1} at 900 °C. Moreover A-site lanthanum doping improves the electronic conductivity but shows low ionic conductivity and poor catalytic activity. Low catalytic activity can be improved by infiltration of various transition metal and metal oxides such as Cu, Ni and CeO_2[16, 19, 20]. It is shown that presence of Ni and CeO_2 in $LSCT_{A-}$ backbone decreases the polarization losses and provides the stable performance of the cell during redox cycling[21].

In the present work, using environment friendly, aqueous processes, an A-site deficient $LSCT_{A-}$ anode backbone is fabricated, characterized and used in YSZ electrolyte supported SOFC. Co-sintering of $LSCT_{A-}$ and dense YSZ has successfully done and as fabricated electrolyte and electrodes layers is perfectly adhered to each other after sintering at 1350 ℃. The aqueous tapecasting along with co-sintering is the novelty of the present work towards direct methane SOFC operation. Aqueous tapecasting is an environment friendly technique as it does not require any toxic solvent. $LSCT_{A-}$ backbone is impregnated with nitrate precursors of Ni and/or CeO_2 to increase the catalytic activity and the cell performances have been determined in H_2 and dry CH_4 at 800 °C. As discussed earlier that YSZ electrolyte does not

react with LSCT$_{A-}$ under normal co-sintering. To avoid reaction between cathode and electrolyte during sintering of fabricated cell, the cathode is impregnated with the catalyst in pre-sintered YSZ porous scaffold. A 15% LSF-5%LSC-YSZ cathode has been used in all the cells [21]. Finally, current-voltage characteristics obtained is analyzed using anode morphology, structure and electrochemical impedance spectroscopy. The current work explores the potential of La and Ca co-doped A site deficient SrTiO$_3$ anode for direct methane SOFC.

Experimental

Button SOFC cells were fabricated by an environment friendly aqueous tape casting and co-sintering of dense YSZ electrolyte, porous electrodes of LSCT$_{A-}$ anode and YSZ porous scaffold for cathode [16]. The LSCT$_{A-}$ (Topsoe fuel cells) powder for the anode or YSZ powder for cathode were mixed with graphite and milled for 24 h by adding de-ionized water as solvent and hypermer KD 6 as a dispersant. Subsequently, poly(ethylene glycol) and glycerol as plasticizer, polyvinyl alcohol and ethoxylated 2,4,7,9-tetra ethyl 5 decyn-4,7-diol as defoamer were added to the slurry and milled further for 24 h. The suspension was de-aired and cast to produce the green tape. In a similar way, dense YSZ green tapes were fabricated without the addition of graphite. After drying, green tapes were laminated all together to produce porous YSZ/denseYSZ/porous LSCT$_{A-}$ green tape. The green tapes were cut into the appropriate size and co-sintered at 1350 °C for 4 h in air. The active area of the cell was measured to be 0.5 cm^2. The sintered anode was reduced in H$_2$ atmosphere at 950 °C and the color of LSCT$_{A-}$ anode changed from light yellow to bluish black. The YSZ porous scaffold for cathode was impregnated with nitrate precursors of La, Sr and Fe (for La$_{0.8}$Sr$_{0.2}$FeO$_3$, LSF) and La, Sr and Co (for La$_{0.8}$Sr$_{0.2}$CoO$_3$, LSC) successively and calcined at 500 °C in air. The final loading in cathode matrix was 15 wt % LSF and 5 wt % LSC. One of the perovskite phase matched with JCPDS file # 48-0124, which corresponds to La$_{0.7}$Sr$_{0.3}$Co$_{0.3}$Fe$_{0.7}$O$_{3-\delta}$. It might be possible that infiltrated LSF and LSC precursors formed La$_x$Sr$_{1-x}$Co$_y$Fe$_{1-y}$O$_3$ perovskite phase during heat

treatment. Further, the peak at 2θ angle of 25º corresponds to La($Co_{0.42}Fe_{0.58}O_3$) as reported in JCPDS file # 01-074-9369. CeO_2 and/or Ni catalyst were impregnated in $LSCT_{A-}$ porous anode matrix using $Ce(NO_3)_3.6H_2O$ and $Ni(NO_3)_2.6H_2O$ solution[22]. Multiple impregnation and calcination at 500 °C were carried out to get appropriate loading. Silver wires, used as current collectors, were connected to both the electrodes using silver paste. The cell was sealed onto a ceramic tube keeping anode towards the inner side of the tube with the help of Aremco, Ceramabond 552. Reduction environment, 5% H_2-95% N_2 gas mixture was fed into the anode chamber till the operating temperature reached (800 °C) then pure H_2 or dry CH_4 was supplied with a flow rate of 40-50 mL/min. In cathode side, atmospheric air was used as the oxidant. The current-voltage characteristics followed by impedance studies were done using potentiostat/galvanostat (Autolab, Metrohm). The frequency range for impedance spectroscopy was 0.01 Hz to 1 MHz at open circuit voltage (OCV). The microstructure, morphology and elemental mapping of the anode before and after cell operation had been analyzed by scanning electron microscope (SEM) and energy dispersive x-ray spectroscopy (EDX) using Zeiss EVO 50. The particle size and selected area diffraction patterns were observed using high resolution transmission electron microscope (HR-TEM) by Technai G^2 200 KV, FEI. The phase purity and crystallite size of a constituent of the electrode had been analyzed using X-ray diffraction (XRD) (PW 2040/60, X'Pert PRO, Netherland) before and after cell testing.

Results and Discussion

Physical Characterization of $LSCT_{A-}$ Anode

The sintered $LSCT_{A-}$ anode pellet analyzed using SEM is shown in fig. 1 (a-d). It is observed in fig. 1a that $LSCT_{A-}$ pellet has well-sintered grains with sufficient porosity (33%). The porosity value of 30-40% in anode is sufficient to provides high contact surface between the gas phase and anode-electrolyte material as well as shorten the diffusional length[23]. In the

present case the porosity is ~33%, which is estimated using Archimedes' principle after sintering of the anode.

Terrace like feature is observed in fig. 1 (b), which is the characteristics feature of A-site deficient $SrTiO_3$ perovskites[24]. Average particle size is found to be ~5 μm. Morphological and elemental analyses of $LSCT_{A-}$ anode pellets reduced at 800 and 950 °C are presented in fig. 1 (c-d). SEM analyses show well patterns $LSCT_{A-}$ backbone grains with sufficient porosity and structural stability. The average particle size of reduced $LSCT_{A-}$ is ~5 μm. Terrace like pattern, which is observed in unreduced $LSCT_{A-}$ (fig. 1b) pellet, is still present in reduced $LSCT_{A-}$ pellet. Fig. 2 presents SEM and corresponding elemental mapping through EDX of reduced $LSCT_{A-}$ anode pellet. Elemental mapping shows a uniform distribution of constituents throughout the $LSCT_{A-}$ backbone structure. Further, EDX analysis confirmed the presence of La, Sr, Ca, Ti and O in the backbone structure. HR-TEM of reduced $LSCT_{A-}$ pellet is shown in fig. 3 (a-b). Fig. 3a shows HRTEM of $LSCT_{A-}$ at lower magnification. In fig. 3a the surface of $LSCT_{A-}$ can be seen and inset of fig. 3a shows grains of $LSCT_{A-}$. Fig. 3b is the magnified view of fig. 3a, where fringes correspond to $LSCT_{A-}$ is observed. The homogenous lattice patterns in the HRTEM and the regular crystal diffraction pattern in the selected area electron diffraction (SAED) seen in inset of fig. 3b indicate the crystalline nature and regular shape of $LSCT_{A-}$ particles.

Fig. 4 shows XRD pattern of unreduced and reduced sintered $LSCT_{A-}$ pellets. Most of the diffraction peaks correspond to cubic symmetry. Positions of all the peaks are almost unchanged in reduced and unreduced samples, which indicate that composition retained its perovskite structure and no extra peaks are observed. It has been observed that A-site deficient $La_{0.2}Sr_{0.7}TiO_3$ exhibits cubic symmetry [16, 25] but Ca^{2+} doping to lanthanum strontium titanates reduces the symmetry from cubic through tetragonal to orthorhombic. The replacement of larger Sr^{2+} (1.44 Å) with smaller size Ca^{2+} (1.35 Å) is likely to increase the distortion of

perovskite structure by decreasing the tolerance factor from 0.948 to cubic $LSCT_{A-}$ to 0.932 for orthorhombic $LSCT_{A-}$[16]. The peak at 38.4 (121) indicates the structure change from ideal cubic to lower symmetry. During reduction of Ti^{4+} (0.60 Å) to Ti^{3+} (0.67 Å) removing oxygen anions from the lattice could result in the decrease of the lattice parameter.

Cell testing

Electrolyte supported cell (15%LSF-5%LSC-YSZ/YSZ/$LSCT_{A-}$) with $LSCT_{A-}$ anode is tested in H_2 and CH_4 fuels at 800 °C for 7 h to assess the electrocatalytic activity of $LSCT_{A-}$. Fig. 5 shows the impedance analysis of the cell. Initially, at 800 °C, the cell shows 0.76 and 0.26 ohm cm^2 ohmic and polarization resistances in H_2. A decrease in polarization loss at OCV is observed with cell operation time. Impedance analyses at OCV suggest that as exposure to H_2 increases, the resistance decreased and resulted in improved performance. Initially, the cell is operated in H_2 fuel at 800 °C for 3 h. The improvement in cell performance indicates that the reduction of $LSCT_{A-}$ is still going on in H_2 atmosphere giving an enhanced catalytic activity of anode. To distinguish the impedance spectra, plots correspond to cell run between 0-3 h in H_2 is shown in inset of fig. 5b. After 3 h in H_2, dry CH_4 is supplied as fuel to the anode side. After the cell is operated in dry CH_4 for 3 h at 800 °C, CH_4 is replaced by H_2. Coking did not affect the cell performance. Although the ohmic resistance in dry CH_4 is comparable to that H_2 atmosphere but polarization losses are almost doubled. After testing in CH_4, improvement in performance is observed in H_2 at 7 h of operation. The ohmic resistance is unchanged but the polarization resistance has been reduced from initial value 0.26 to 0.16 ohm cm^2. The polarisation resistance in the present study is 0.20 ohm cm^2, which is much lower than the reported value 1.86 ohm cm^2 [22, 26]. It can be inferred from above mentioned analyses that $LSCT_{A-}$ is catalytically not very active for methane decomposition but it does not promote the coke deposition during operation as evident from the stable performance after dry CH_4 exposure for 3 h. The low CH_4 fuel utilization i.e. 2 % in case of complete oxidation and 8 %

in case of partial oxidation at 800 °C in SOFC test condition is observed. Therefore the porous LSCT$_{A-}$ anode is impregnated with an active material to increase the catalytic activity in CH$_4$ fuel and they are discussed below.

To enhance the catalytic activity in CH$_4$, 6% CeO$_2$ is impregnated to porous LSCT$_{A-}$ anode and tested in electrolyte supported cell (15%LSF-5%LSC-YSZ/YSZ/6%CeO$_2$-LSCT$_{A-}$) in H$_2$ and dry methane at 800 °C. It is observed from impedance analyses at OCV, shown in fig 6, that ohmic (0.69 to 0.72 ohm cm^2) as well as polarisation resistance does not change significantly in H$_2$ between 0-3 h, which might be due to the better interconnection between CeO$_2$ particles on LSCT$_{A-}$ backbone. The presence of CeO$_2$ enhances the ionic conductivity in anode backbone. After 3 h of operation in dry CH$_4$, ohmic resistance increased to 0.77 from 0.69 ohm cm^2 in H$_2$ fuel at 7 h of cell operation. The lower performance of the cell in CH$_4$ is due to sluggish reaction associated with the dissociation of CH$_4$. The polarisation resistance at 0 h and 3 h are 0.13 and 0.12 ohm cm^2 and even after 3h of CH$_4$ exposure the polarisation resistance in H$_2$ at 7 h is only 0.14 ohm cm^2. Negligible loss (0.01 ohm cm^2) in polarisation resistance indicates that performance degradation under dry CH$_4$ is not drastic after CeO$_2$ is added to LSCT$_{A-}$. Impedance spectra correspond to cell run in H$_2$ before and after CH$_4$ exposure is presented in inset of fig. 6.

Morphological and elemental analysis of the cell after 7 h of operation is presented in fig. 7(a-d). The thickness of the anode, electrolyte and cathode are 100, 300 and 100 μm, respectively, as shown in fig 7a. The electrolyte is dense and adhered properly to both the porous electrodes and no delamination or cracks have been observed. The uniform distribution of CeO$_2$ particles on LSCT$_{A-}$ backbone is seen from fig. 7b. The presence of a constituent element is confirmed by EDX analysis of anode matrix after the operation as shown in fig 7c. Proper adherence between cell components as shown in fig. 7a as well as stable electrodes presented in fig. 7b and 7d after cell testing indicate that aqueous tapecasting and co-sintering method provide

robust structure, which can sustain CH_4 exposure during accelerated testing at 800 ºC. It may be noted that porosity and morphology can be controlled using aqueous tapecasting. The presence of some cobalt is observed, which may be due to spillover from cathode matrix during impregnation. In present work the spillover of Co from cathode side to anode is too low to affect the performance. The role of Co in anode is not studied but it is reported that infiltration or doping of Co enhance the performance of Ni based anode [27-28]. The presence of carbon on $LSCT_{A-}$ backbone is due to the decomposition of dry CH_4 during cell operation (fig. 7 d). The uniform distribution of constituent elements in anode matrix is noted from the SEM and elemental mapping presented in fig. 7d.

To increase the performance of catalytic activity of $LSCT_{A-}$ anode matrix further 4% Ni is impregnated along with 6% CeO_2. The current-voltage performance of the electrolyte supported cell (15%LSF-5%LSC-YSZ/YSZ/6%CeO_2-4%Ni-$LSCT_{A-}$) at 800 °C in H_2/CH_4 and impedance analysis are shown in fig. 8 (a-b). The maximum power density obtained is 310 mW cm^{-2} (636 mA cm^{-2}) initially, which increases up to 328 mW cm^{-2} (652 mA cm^{-2}) in H_2 at 3 h of cell operation due to continuous reduction of anode active material. The improvement in performance indicates that the Ni particles in the presence of CeO_2 are not agglomerated due to sintering at elevated temperature. This may suggest strong metal support interaction (SMSI) between Ni and CeO_2 preventing coarsening of Ni [29]. A similar behavior between Ni and TiO_2 on YSZ backbone has been reported earlier [9-10]. After cell operation in H_2, dry CH_4 fuel is fed into the anode chamber. The maximum power density obtained is 250 mW cm^{-2} (495 mA cm^{-2}) in CH_4, which is less than that of the performance shown in H_2. The performance of the cell degraded significantly in 3 h of operation in dry CH_4 exposure. The maximum power density reduced to 165 mW cm^{-2} (309 mA cm^{-2}) after 3 h of cell testing in dry CH_4, which is half of the performance shown by the cell in H_2. The degradation in performance is due to the coke deposition in active sites (Ni) of the anode. The degradation in performance may be arrested if

humidified CH_4 fuel is used. It is observed from impedance plot in Fig 8b that between 0-3 h of cell operation in H_2, the ohmic resistance is almost constant whereas polarization resistance at OCV reduces with time. The ohmic resistance in the presence of dry CH_4 decreased to 0.56 ohm cm^2 from that of 0.62 ohm cm^2 in H_2 after 3 h of operation. With the increase in operation time, the ohmic resistance increases in dry CH_4 but still lower than that obtained in H_2. The decrease in ohmic resistance may be due to deposition of carbon in the interstices of anode particles. In inset of fig.8b impedance corresponds to operation in H_2 is presented to distinguish the spectra.

Figure 9 (a-d) represents the morphology, EDX and elemental analyses of the cell components after 7 h operation. Well-connected fine particles of LSF and LSC cathode catalysts in pores of YSZ are observed from SEM micrographs in fig. 9a. The average particle size in the cathode is ~100 nm. SEM micrograph (fig. 9b) shows the dispersed Ni/CeO_2 in the pores of $LSCT_{A-}$ anode. It is difficult to distinguish between Ni and CeO_2 but from earlier observation, it may be inferred that visibly significant presence of crystal particles represents Ni. The average particle size of Ni/CeO_2 impregnated $LSCT_{A-}$ anode catalyst is between 100-200 nm and there is no agglomeration of Ni is observed. The constituents of Ni/CeO_2 impregnated $LSCT_{A-}$ anode matrix is confirmed by the EDX analysis as shown in fig. 9c. The elemental mapping confirmed the uniform distribution of different elements throughout the anode matrix (Fig. 9d).

After cell operation Ni-CeO_2-$LSCT_{A-}$ anode is separated out and a suspension of particles is prepared in isopropanol to carry out HR-TEM analysis. HR-TEM, EDX and SAED patterns of anode after cell operation are presented in fig. 10(a-c). No change in morphology of the anode material is observed after cell operation. A well-dispersed Ni/CeO_2 particles in $LSCT_{A-}$ is observed in fig. 10a. The diffraction pattern corresponding to crystalline nature of $LSCT_{A-}$ is shown in the fig. 10b. EDX confirmed the presence of La, Sr, Ca, Ti, O, Ni and Ce in the anode (fig. 10c). The peak corresponds to Cu is due to the Cu-grid used during analysis. By comparing

SAED of fig. 3b and fig. 10d, it is observed that other than regular crystal diffraction pattern, a separate pattern correspond to Ni/CeO$_2$ is also present. XRD pattern corresponds to Ni/CeO$_2$ impregnated LSCT$_{A-}$ anodes have been shown in fig. 11. The peaks correspond to LSCT$_{A-}$, CeO$_2$ and Ni/NiO are identified. No alloy formation between impregnated catalysts and LSCT$_{A-}$ is observed. The unique perovskite structure of LSCT$_{A-}$ remains intact with no change in impregnated CeO$_2$ and Ni/NiO after cell testing. A small shift in peaks position towards lower angle and additional peaks of Ni have been observed in anode after SOFC operation, which may be due to change in microstructure during reduction at elevated temperature. The average crystallite size of LSCT$_{A-}$ anode estimated using scherrer formula ($t = K\lambda/\beta\cos\theta$, where t is the crystallite size, K is the dimensionless shape factor, λ is the wavelength of Cu Kα, 1.54 Å, β is the full width at half maxima and θ is the bragg angle in degrees) is 65 nm.

Conclusion

Environment friendly aqueous tapecasting followed by co-sintering of green tape has been successfully implemented to fabricate button cells. Aqueous tapecasting provided porous and stable LSCT$_{A-}$ electrode and dense YSZ electrolyte. Electrolyte supported solid oxide fuel cell with LSCT$_{A-}$ anode is tested in H$_2$ and dry CH$_4$ fuel. LSCT$_{A-}$ works reasonably well in H$_2$ fuel but exhibited low performance in dry CH$_4$. However, 6% CeO$_2$ impregnated in the LSCT$_{A-}$ backbone anode shows significant improvement in performance of the electrolyte supported cell in H$_2$ and CH$_4$ at 800 °C. It is observed that coke deposition in 6% CeO$_2$ impregnated in the LSCT$_{A-}$ anode is not detrimental to CH$_4$ oxidation. In order to improve the performance of the cell in dry methane, 4% Ni is infiltrated in 6% CeO$_2$-LSCT$_{A-}$ anode. Although performance improved from 194 to 328 mWcm^{-2} at 800 °C for H$_2$, a similar improvement in performance is not observed in dry CH$_4$. Initial performance in dry methane is 250 mW cm^{-2}, which reduces to 165 mW cm^{-2} in 3 h. Ni may have accelerated the coke deposition at the active sites resulting

loss in performance. Nevertheless, a maximum power density of 165 mW cm^{-2} is maintained even after 3 h of operation in dry CH_4. It may be noted that the performance of the cell is reasonably good for a cell with electrolyte thickness of 300 μm. Thus, 4% Ni in combination with 6% CeO_2 enhances the cell performance and the catalytic activity of LSCT$_{A-}$ anode towards oxidation of CH_4 can be recommended as active anode catalysts for direct CH_4 SOFC.

References

1. R. J. Gorte and J. M. Vohs, J. Catalysis, **216**, 477 (2003).

2. R. J. Gorte, S. Park, J. M. Vohs and C. Wang, Adv. Mater., **12**(19), 1465 (2000).

3. H. Kim, S. Park, J. M. Vohs and R. J. Gorte, J. Electrochem. Soc., **148**(7), A693 (2001).

4. H. Kim, C. Lu, W. L. Worrell, J. M., Vohs and R. J., Gorte, J. Electrochem. Soc., **149**, A247 (2002).

5. S. K. Lee, A. Kipyung, J. M. Vohs and R. J. Gorte, Electrochem. and Solid-State Letters, **8**, A48 (2005).

6. G. Kaur and S. Basu, J. Power Sources, **241**, 783 (2013).

7. G. Kaur and S. Basu, Fuel cells, **14**(6), 1006 (2014).

8. G. Kaur and S. Basu, Int. J. Energy Res., **39**, 1345 (2015).

9. C. A. Singh, L. Bansal, P. Tiwari and V. V. Krishnan, ECS trans., **25**(2), 897 (2009).

10. P. Tiwari and S. Basu, Int. J. Hydrogen Energy, **38**, 9494 (2013).

11. P. Tiwari and S. Basu, J. Solid State Electrochem., **18**:805 (2014).

12. P. Tiwari and S. Basu, ECS Trans., **57**(1), 1545 (2013).

13. C. Sun and U. Stimming, J. Power Sources, **171**, 247 (2007).

14. S. Tao and J. T. S. Irvine, J. Mater. Chem., **12**, 2356 (2002).

15. S. W. Tao and J. T. S. Irvine, Chemical Record, **4**(2**),** 83 (2004).

16. A. D. Aljaberi and J.T.S. Irvine, J. Mater. Chem. A, **1**, 5868 (2013).

17. C. D. Savaniu and J.T.S. Irvine, Solid State Ionics, **192**, 491 (2011).

18. P. Tiwari and S. Basu, ECS Trans., **68** (1), 1435 (2015).

19. A. Yaqub, C. D. Savaniu, N. K. Janjua and J. T. S Irvine, J. Mater. Chem. A, **1**, 14189 (2013).

20. P. Tiwari, J. T. S. Irvine and S. Basu, ECS Trans., **78** (1), 1195 (2017).

21. M. C. Verbraeken, B. Iwanschitz, A. Mai and J. T. S. Irvine, J. Electrochem. Soc., **159** (11), F757 (2012).

22. L. Lu, M. C. Verbraeken, M. Cassidy and J. T. S. Irvine, ECS Trans., **57**(1), 1415 (2013).

23. W.Z. Zhu and S.C. Deevi, Mater. Sci. and Engin., **A362,** 228 (2003).

24. D. Neagu and J. T. S. Irvine, Comprehensive Inorganic Chemistry II, 397 (2013).

25. C. D. Savaniu and J.T.S. Irvine, J. Mater. Chem., **19**, 8119 (2009).

26. L. Lu, C. Ni, M. Cassidy and J.T.S. Irvine, J. Mater. Chem., **4**, 11708 (2016).

27. T. Guo, X. Dong, M. M. Shirolkar, X. Song, M. Wang, L. Zhang, M. Li, and H. Wang, Appl. Mater. Interfaces **6**, 16131 (2014).

28. S. H. Cui, J. H. Li, X. W. Zhou, G. Y. Wang, J. L. Luo, K. T. Chuang, Y. Bai and L. J. Qiao, J. Mater. Chem. A, **1**, 9689 (2013).

29. J. Qiao, K. Sun, N. Zhang, B. Sun, J. Kong and D. Zhou, J. Power Sources, **169**, 253 (2007).

List of Figures

Fig. 1 SEM micrographs (a) lower magnification, (b) higher magnification of unreduced LSCT$_{A-}$ pellet sintered at 1350 °C in air; SEM micrographs of LSCT$_{A-}$ pellet reduced in H$_2$ atmosphere at (c) 800 °C and (d) 950 °C.
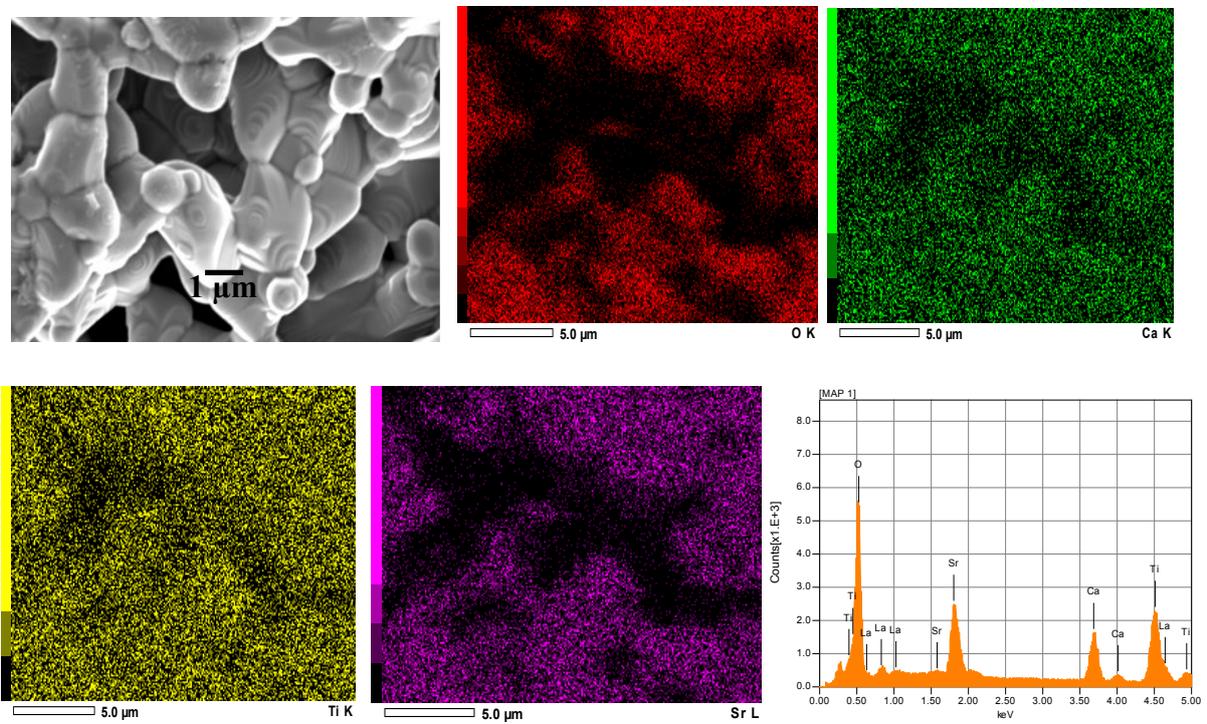
Fig. 2 SEM, Elemental mapping and EDX of reduced LSCT$_{A-}$ pellet.
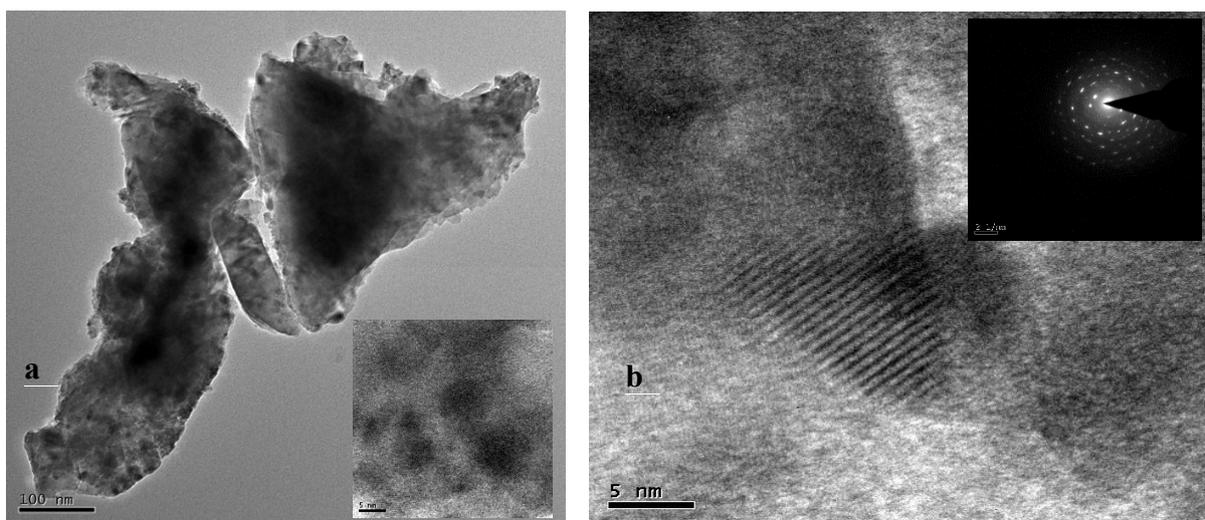
Fig. 3 (a-b) HRTEM Micrograph and SAED of reduced LSCT$_{A-}$ anode.
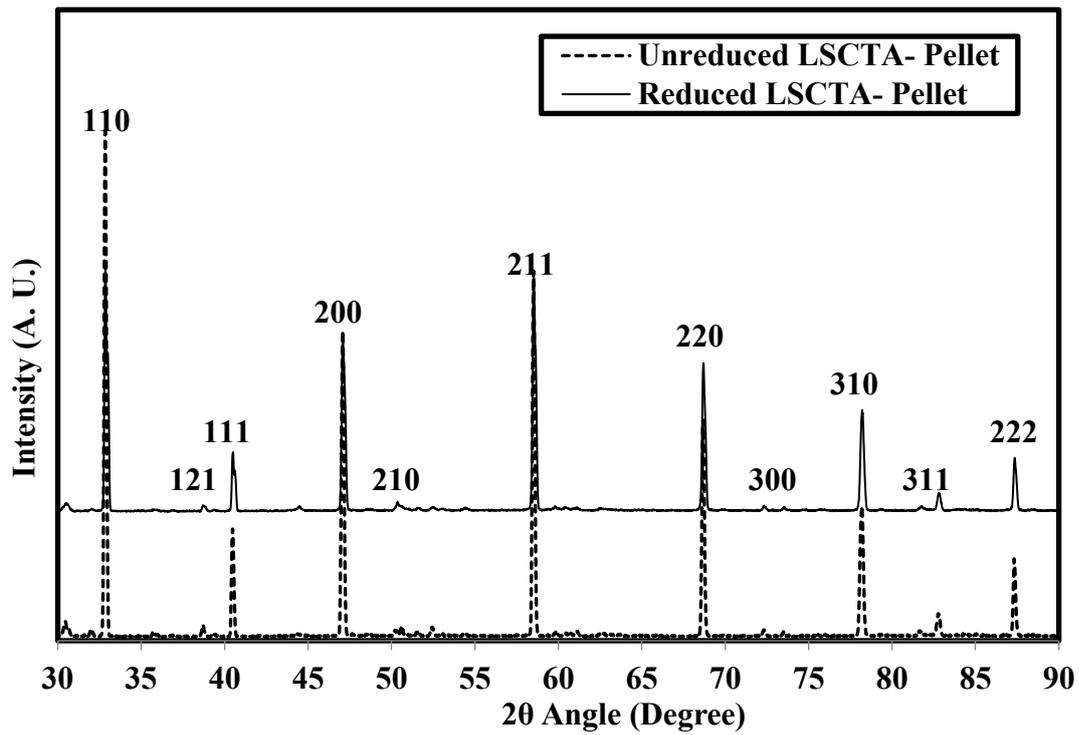
Fig. 4 XRD patterns of sintered LSCT$_{A-}$ anode pellets.
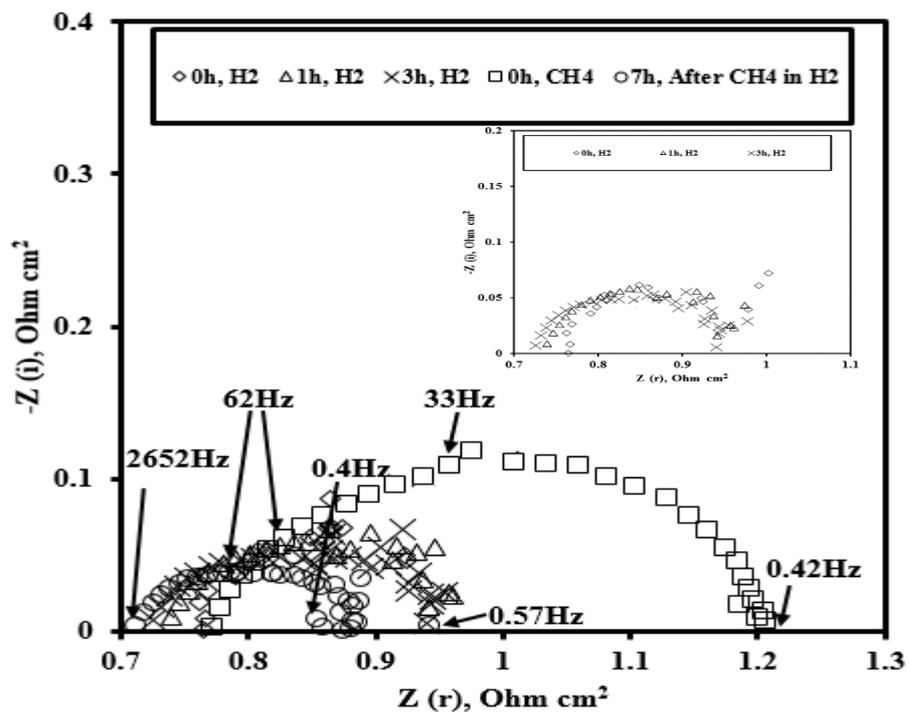
Fig.5 EIS characteristics at OCV of electrolyte supported SOFC (15%LSF-5%LSC-YSZ/YSZ/LSCT$_{A-}$) for 7 h.
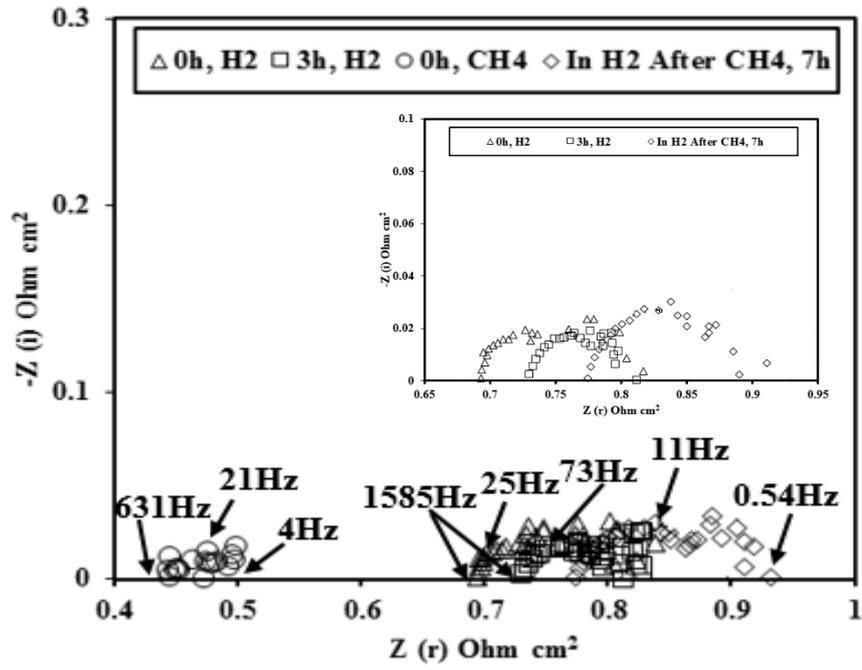
Fig. 6 EIS characteristics at OCV of electrolyte supported SOFC (15%LSF-5%LSC-YSZ/YSZ/6%CeO$_2$-LSCT$_{A-}$) for 7 h.
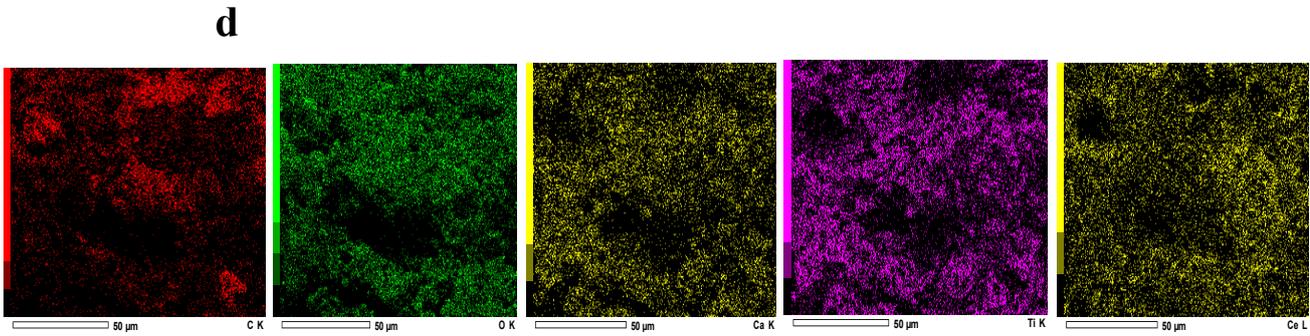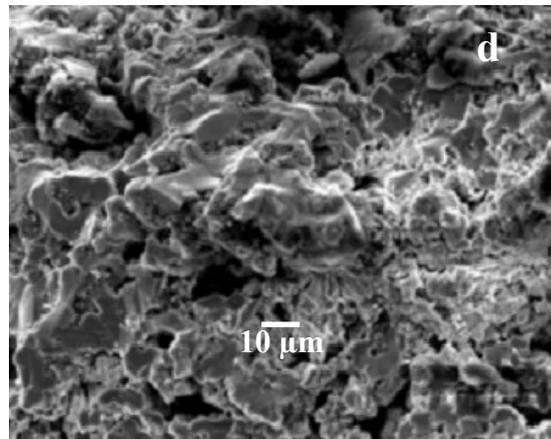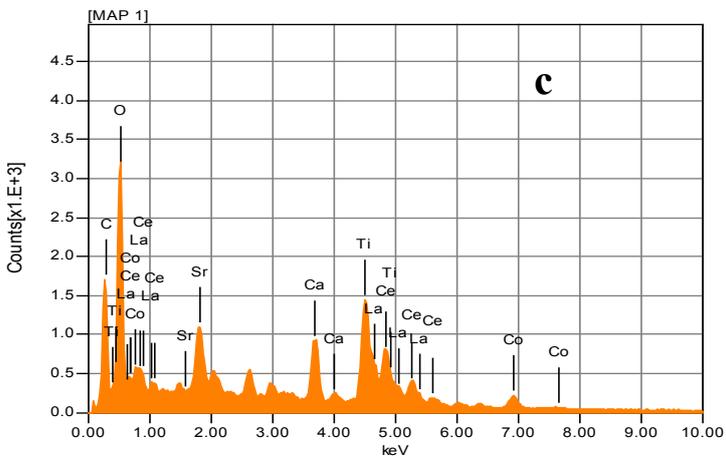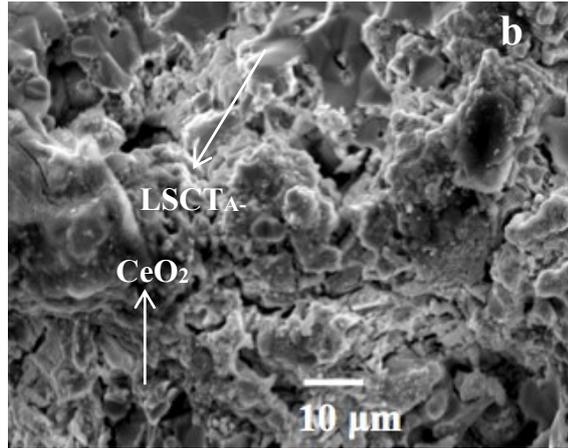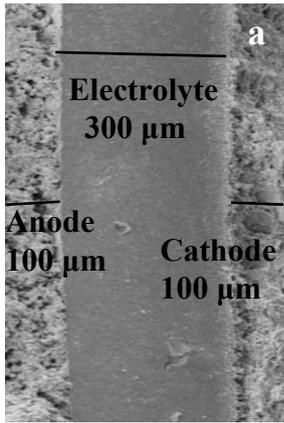
Fig. 7(a) Fracture surface of the cell after operation (b) Morphology (c) EDX (d) SEM and Elemental mapping of $LSCT_{A-}$ anode impregnated with 6%CeO_2 after cell operation of 7 h.
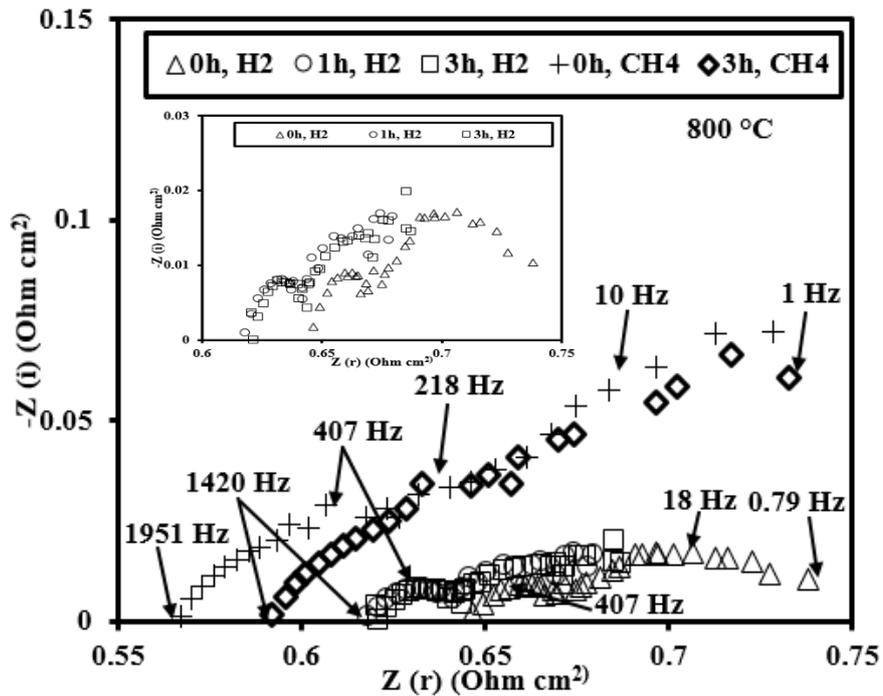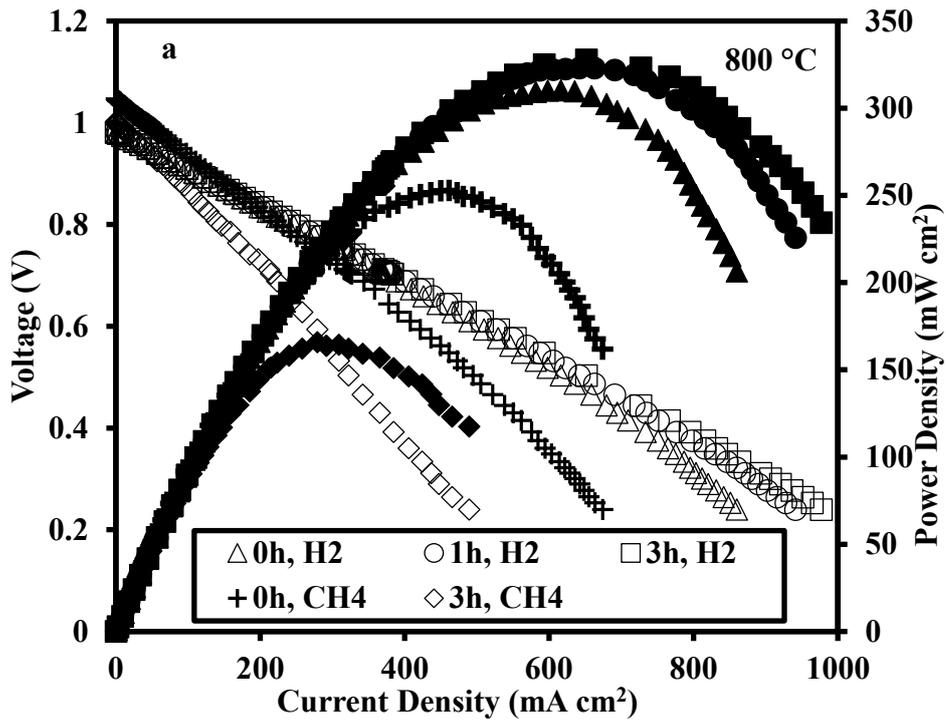
Fig. 8(a) i-V, i-P and (b) EIS characteristics at OCV of electrolyte supported SOFC (15%LSF-5%LSC-YSZ/YSZ/6%CeO$_2$-4%Ni-LSCT$_{A-}$) for 7 h.
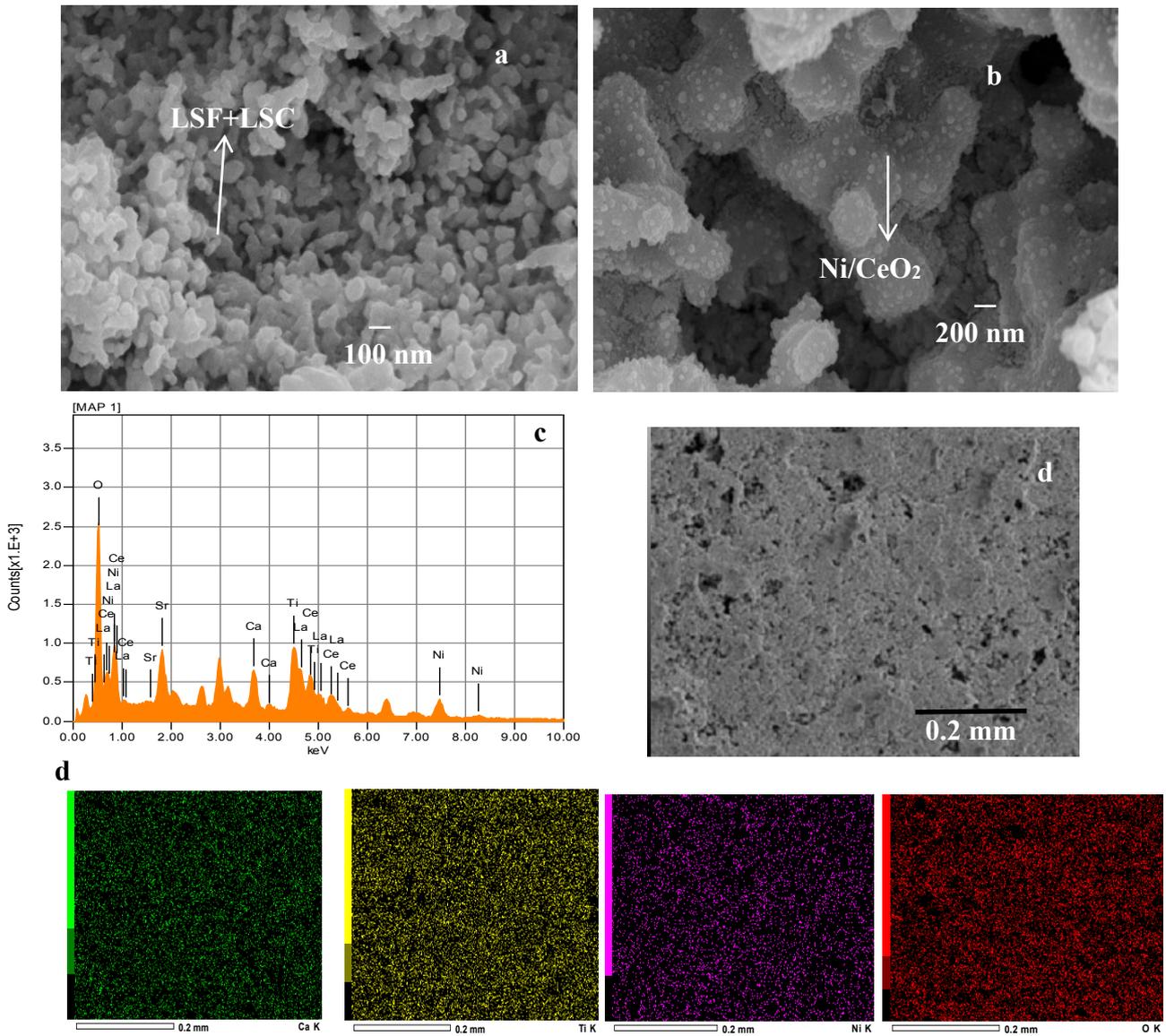
Fig. 9 (a) SEM of porous YSZ cathode matrix impregnated with 15%LSF + 5%LSC, after cell testing (b) Morphology, (c) EDX and (d) SEM and Elemental mapping of LSCT$_{A-}$ anode impregnated with 6% CeO$_2$-4% Ni after cell operation of 7 h.
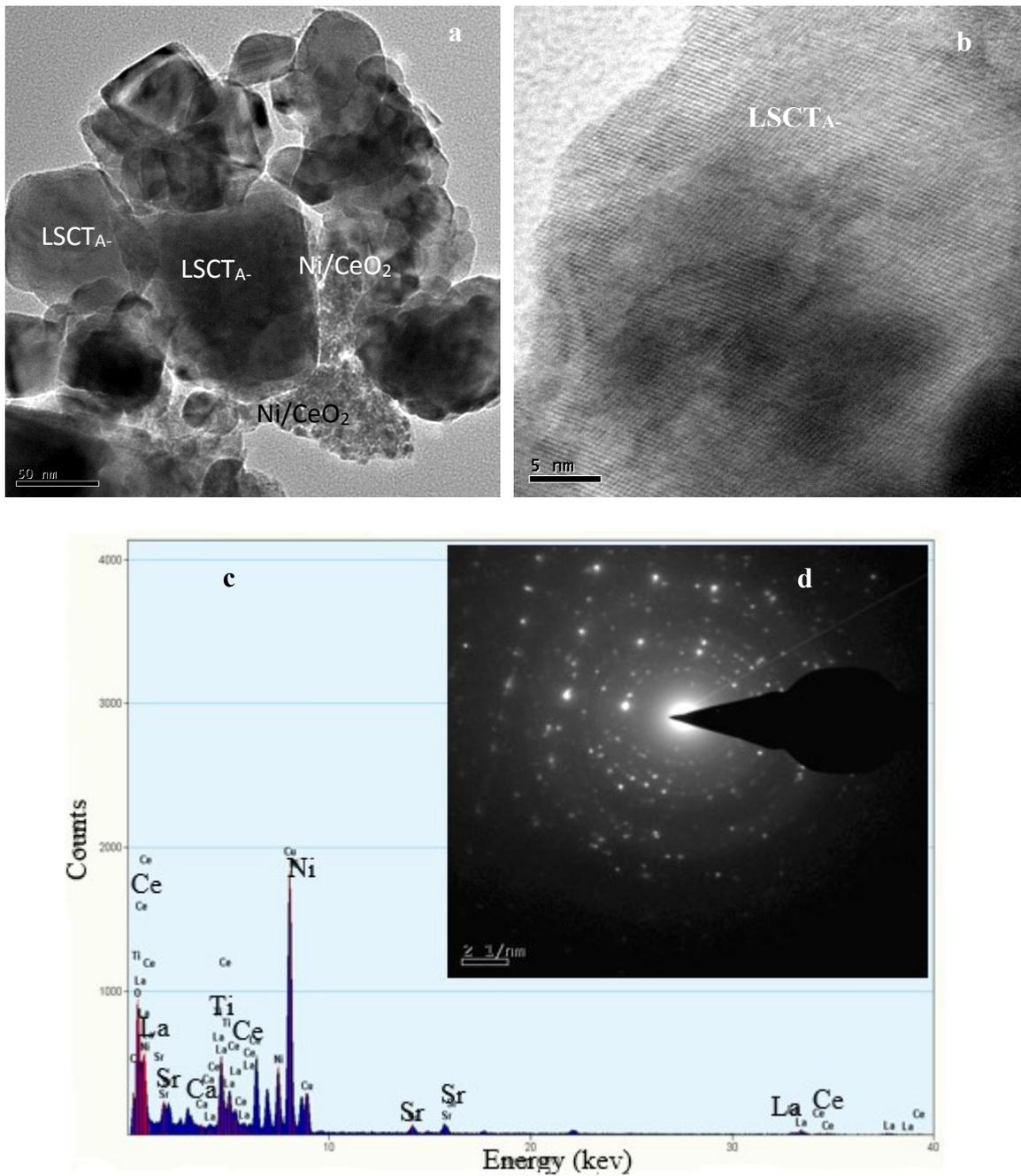
Fig. 10 (a-d) HRTEM, SAED and EDX of LSCT$_{A-}$ anode impregnated with 6%CeO$_2$-4% Ni after cell operation of 7 h.
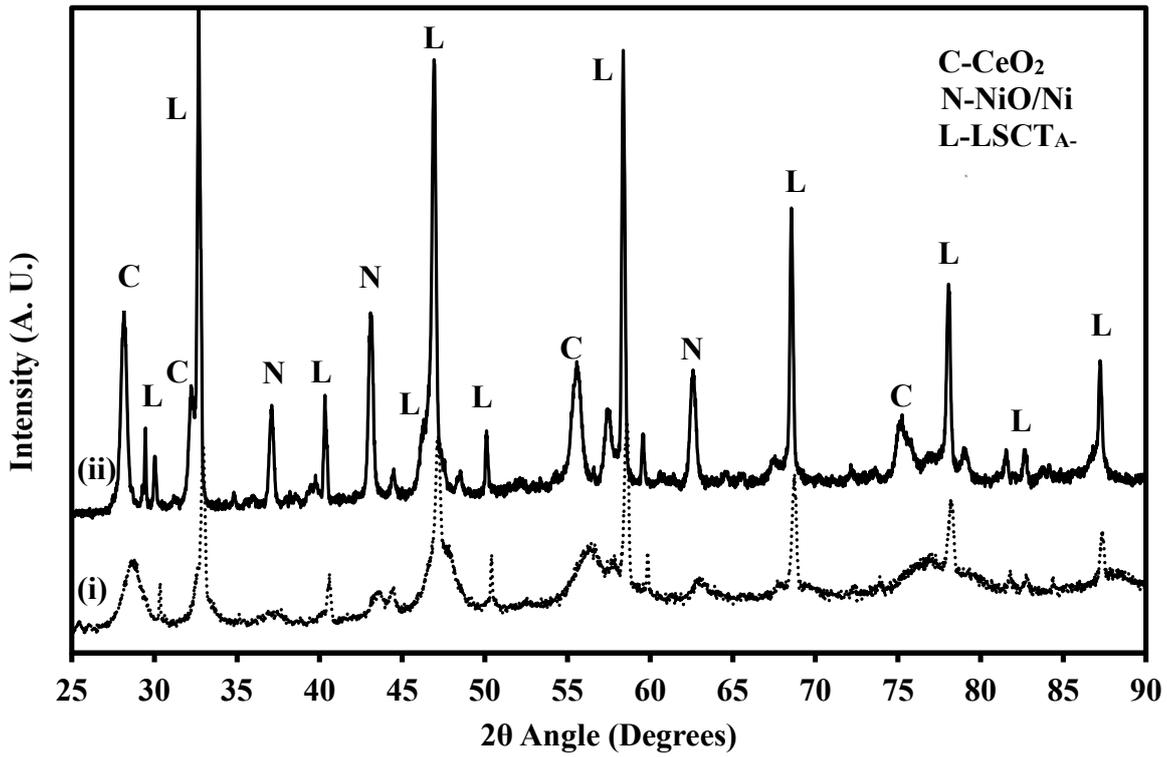
Fig.11 XRD patterns of 6%CeO$_2$-4%Ni-LSCT$_{A-}$ anodes (i) before and (ii) after cell testing.